Structural and Vibrational Properties of Arsenic Sulfides: Alacranite (As8S9)

5 **AUTHORS**, INCLUDING:

P. Bonazzi
University of Florence
76 PUBLICATIONS **732** CITATIONS

SEE PROFILE

Luca Bindi
University of Florence
241 PUBLICATIONS **1,423** CITATIONS

SEE PROFILE

Maurizio Muniz-Miranda
University of Florence
202 PUBLICATIONS **2,085** CITATIONS

SEE PROFILE

Gianni Cardini
University of Florence
171 PUBLICATIONS **2,373** CITATIONS

SEE PROFILE

# Structural and Vibrational Properties of Arsenic Sulfides: Alacranite (As_8S_9)

Marco Pagliai,[†] Paola Bonazzi,[‡] Luca Bindi,[§] Maurizio Muniz-Miranda,[†,∥] and Gianni Cardini[*,†,∥]

[†]Dipartimento di Chimica "Ugo Schiff", Università degli Studi di Firenze, Via della Lastruccia 3, 50019 Sesto Fiorentino (Firenze), Italia

[‡]Dipartimento di Scienze della Terra, and [§]Museo di Storia Naturale, Sezione di Mineralogia, Università degli Studi di Firenze, via La Pira 4, 50121 Firenze, Italia

[∥]European Laboratory for Non-Linear Spectroscopy (LENS), via Nello Carrara 1, 50019 Sesto Fiorentino (Firenze), Italia

ABSTRACT: Alacranite, As_8S_9, has been studied by a combined approach based on micro-Raman measurements and *ab initio* molecular dynamics simulations, with the Car—Parrinello method. The structure of this arsenic sulfide mineral consists of an ordered packing of As_4S_4 and As_4S_5 cagelike molecules, with a topology closely resembling that found in the β-As_4S_4. The presence in the crystal structure of molecular clusters with permanent dipole moment induces stronger intermolecular interactions than those observed in other arsenic sulfides, making the adoption of *ab initio* computational methods particularly important for a complete characterization of the structural and spectroscopic properties.
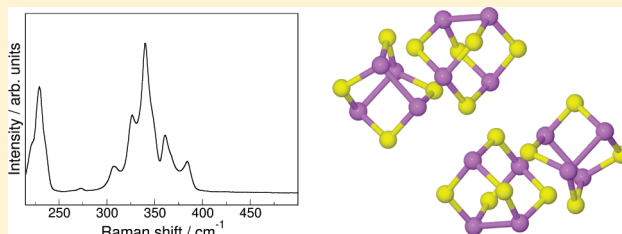
INTRODUCTION

Because of the high degree of specificity, excellent spatial resolution, and relatively high sensitivity, micro-Raman spectroscopy have been revealed particularly effective in the characterization of materials with interest in Earth and planetary sciences,[1] as well as in nondestructive *in situ* identification of pigments in artistic and historic artworks (e.g., Trentelman et al.[2]). Realgar and naturally occurring arsenic sulfide minerals are brightly colored and consequently have been used as pigments since ancient times. When exposed to visible light, unprotected realgar gradually transforms to pararealgar. The proposed light induced reaction mechanism reported in the literature[3−10] occurs in two-steps, with an intermediate formation of the uzonite-type As_4S_5 molecule.

During the initial photoreaction step, the realgar-type (r-type) As_4S_4 molecule transforms to the uzonite-type As_4S_5 molecule according to the oxidation reaction: $5As_4S_4$ (r-type) $+ 3O_2 \rightarrow 4As_4S_5 + 2As_2O_3$. The process goes on through the release of a sulfur atom by breaking an As—S—As linkage to form a para-realgar-type (p-type) As_4S_4 molecule: $As_4S_5 \rightarrow As_4S_4$ (p-type) $+ S$. The molecular structures of realgar-type As_4S_4, pararealgar-type As_4S_4, and uzonite-type As_4S_5 are shown in Figure 1.

The above overall reaction can be monitored by means of both X-ray diffraction[4,6−12] and Raman[2,13] measurements; however, the accurate comprehension of the mechanism is hampered by the fact that no Raman data of compounds containing the uzonite-type molecule have been reported to date. The unusual cohabitation of two different kinds of discrete arsenic sulfide clusters in the structure of alacranite, As_4S_4 (r-type) and As_4S_5, respectively, makes this mineral an ideal case study to this purpose. Moreover, the study of the vibrational properties is of

fundamental relevance for understanding the character of the intermolecular interactions in this mineral, usually attributed to van der Waals interactions.[5,14] Alacranite, As_8S_9, crystallizes in the $P2/c$ space group, with $a = 9.942(4)$ Å, $b = 9.601(2)$ Å, $c = 9.178(3)$ Å, $\beta = 101.94(3)°$, $V = 857.1(5)$ Å^3, and $Z = 4$.[15] The structure, shown in Figure 2, contains two different kinds of cagelike molecules, with a molecular packing closely resembling that found in the β-As_4S_4 (β-phase).[16] The first one is identical to the As_4S_4 molecule found in the structures of both the realgar[17] and β-phase.[16] The other molecule is chemically and structurally identical to that found in the synthetic As_4S_5 compound[18] and in uzonite.[3]

In the present article, we report structural and vibrational properties of alacranite obtained combining micro-Raman measurements and Car—Parrinello molecular dynamics (CPMD)[19−22] simulations. Raman interpretation has been made possible by static or dynamic *ab initio* calculations, especially within the density functional theory (DFT) approach. Recently Pagliai et al.[23] have generalized the method to compute the polarizability tensor proposed by Putrino et al.,[24] allowing one to obtain Raman spectra for cells of any symmetry, starting from trajectories generated by CPMD simulations performed in the same experimental thermodynamic conditions.

COMPUTATIONAL DETAILS

The CPMD simulations[25] of the alacranite crystal have been performed for one unit cell using the BLYP exchange and

ACS Publications   © XXXX American Chemical Society

A

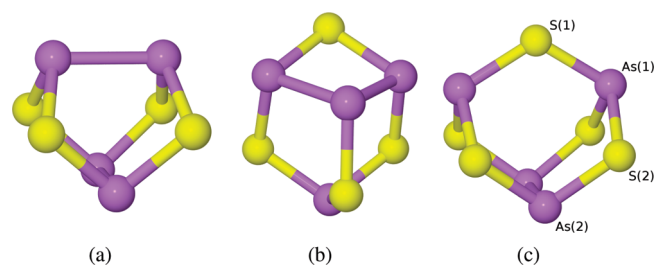dx.doi.org/10.1021/jp201097k | *J. Phys. Chem. A* XXXX, XXX, 000–000

Figure 1. Molecular structure of realgar-type As$_4$S$_4$ (a), pararealgar-type As$_4$S$_4$ (b), and uzonite-type As$_4$S$_5$ (c). The symmetry of realgar and pararealgar As$_4$S$_4$ molecules is D_{2d} and C_s, respectively, whereas the molecular symmetry of As$_4$S$_5$ is C_{2v}. The asymmetric unit in the uzonite-type molecule has been labeled. Yellow and violet spheres refer to sulfur and arsenic atoms, respectively.
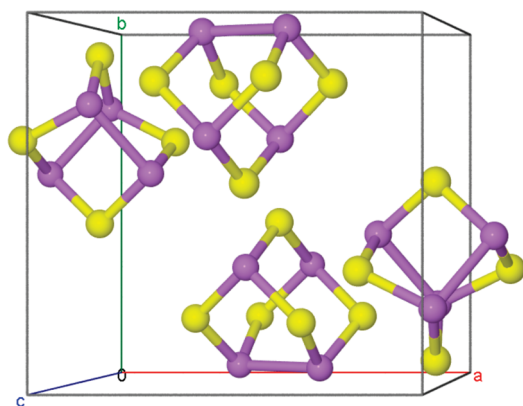

Figure 2. Crystal structure of alacranite, As$_8$S$_9$. Yellow and violet spheres refer to sulfur and arsenic atoms, respectively.

correlation functional,[26,27] starting from the structural data reported by Bonazzi et al.[15] Goedecker–Teter–Hutter (GTH) pseudopotentials[28–30] have been adopted to describe the core region of all elements, and the plane wave expansion has been truncated at 100 Ry in the Γ point, (0,0,0), approximation. The effect of the k-points has been checked performing geometriy optimizations adopting two different Monkhorst–Pack[31] meshes: $2 \times 2 \times 2$ and $3 \times 3 \times 3$. The root-mean-square displacement (rmsd) values for the calculated atomic positions with respect to the experimental ones result in 5.95×10^{-2}, 6.31×10^{-2}, and 6.34×10^{-2} Å for Γ point, $2 \times 2 \times 2$ and $3 \times 3 \times 3$ k-point meshes, respectively. Taking into account the dispersion forces with the approach proposed by Grimme,[32] the geometry optimization gives rise to a rmsd value of 7.58×10^{-2} Å.

The simulation run has been carried out for 131 072 steps, with an integration time step of 5 au (0.12 fs) for a total simulation time of ~15 ps in the microcanonical (NVE) ensemble (the resulting average temperature is ~275 K). The Raman spectrum of the alacranite crystal has been obtained by computing the polarizability tensor with the procedure described in Pagliai et al.[23] for 4096 equispaced configurations extracted from the CPMD trajectory.

■ EXPERIMENTAL DETAILS

Raman spectra of alacranite crystal at ambient conditions were collected using a Renishaw RM2000 micro-Raman apparatus, coupled with a diode laser source emitting at 785 nm. Sample
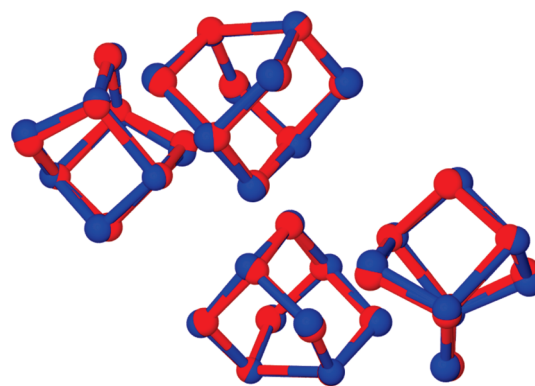

Figure 3. Calculated average structure (blue) compared with the structure obtained by X-ray diffraction experiments (red).[15] The rmsd value is 0.16 Å.

irradiation was accomplished using the $50\times$ microscope objective of a Leica Microscope DMLM. The beam power was about 3 mW, and the laser spot size was adjusted between 1 and 3 μm. Raman scattering was filtered by a double holographic notch filter system and collected by an air-cooled CCD detector. The acquisition time for each measurement was 10 s. All spectra were calibrated with respect to a silicon wafer at 520 cm^{-1}.

■ RESULTS AND DISCUSSION

The structural variations observed during the simulation process can be appreciated in Figure 3 by comparing the calculated average atomic positions with those obtained by the X-ray diffraction data.[15] The results show an overall good agreement with the experiments, with only slight differences that can be ascribed to both the limited size of the simulated sample and the not appropriate evaluation of the dispersion forces by the BLYP exchange and correlation functional[26,27] employed in the calculations.

As recently shown by Gibbs et al.,[14] the interactions that determine the stability of the arsenic sulfides molecular crystals, including alacranite, are essentially due to van der Waals forces,[33] in their more extended meaning, that includes Keesom (permanent dipole–dipole interactions) and Debey (permanent dipole–induced dipole interactions) forces as well as London dispersion forces. Gibbs et al.[14] have performed an accurate analysis of the interactions occurring inside the arsenic sulfides crystals but without verifying the van der Waals terms mostly responsible for the stability of these kinds of crystals.

Since the electronic structure evolves in time during CPMD simulation, it is possible to achieve information on the mutual interactions that arise between the molecules in the system. Localizing the Kohn–Sham orbitals in terms of Wannier Functions[21,22,34,35] has been revealed as particularly useful in the study of the intermolecular interactions. The centers of the Wannier functions, which represent the positions of bond electrons and lone pairs, have been actually revealed suitable in the description of the dipole moment of water[36–42] and methanol[43,44] molecules in liquid phases and of the chemical environment effects on such quantity. In Figure 4 is reported a graphical representation of Wannier Function Centers for realgar-type As$_4$S$_4$ and uzonite-type As$_4$S$_5$ molecules, extracted from the optimized structure of the alacranite crystal.

From the analysis of the Wannier Function Centers, it is possible to obtain the dipole moment of each molecule and to
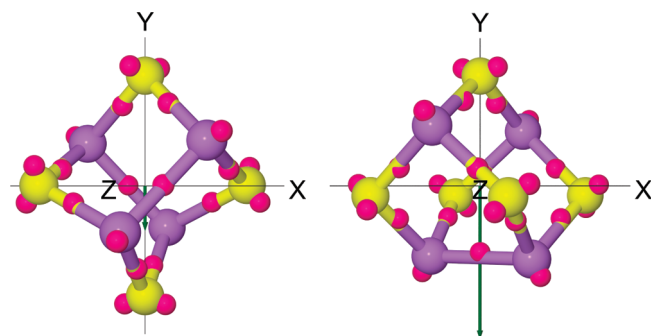
Figure 4. Wannier Function centers (magenta spheres) of realgar-type As_4S_4 and uzonite-type As_4S_5 cages. The molecular dipole moment is reported as a green arrow. Yellow and violet spheres refer to sulfur and arsenic atoms, respectively.

Table 1. Dipole Moment for As_4S_4 and As_4S_5[a]

	A	B	C	D
As_4S_4	0.00	0.05	0.98	1.92 ± 0.67
As_4S_5	0.61	1.04	3.41	3.79 ± 0.91

[a] A, isolated molecule; B, isolated molecule with the same molecular arrangement as in the alacranite crystal; C, molecule in the alacranite crystal; D, average dipole moment and mean square deviation during the CPMD simulation.

follow the variations occurring along with the interactions with the surrounding molecules. The values of the dipole moment for realgar-type As_4S_4 and uzonite-type As_4S_5 molecules are collected in Table 1.

In the case of the isolated molecules, the realgar-type As_4S_4 cage, as a consequence of the D_{2d} symmetry, does not show a molecular dipole moment, whereas the uzonite-type As_4S_5 molecule shows a permanent dipole moment of 0.61 D. This result implies that Keesom and Debey forces have a strong influence on the stability of alacranite structure. The dipole moment of either cages is only slightly affected by the distortion of the molecule in the crystal, while a strong enhancement occurs by moving from isolated molecules to a crystal. The dipole moment of uzonite-type As_4S_5 cage increases until 3.41 D, a value much higher than that observed for the isolated molecule.

The variations of the dipole moment of the molecules in the crystal lattice of alacranite are reported in Figure 5 (the Wannier centers have been computed on 128 equispaced configurations). The panels a and c of Figure 5 show that the Y component of the dipole moment of the uzonite-type As_4S_5 molecules is constantly higher, as the absolute value, than the other components. This behavior is not observed in panels b and d of Figure 5 for the realgar-type As_4S_4 molecule, where the Y component presents only slightly different values. The dipole moment vector for the two molecules, as reported in Figure 4 from the equilibrium configuration of the crystal, is oriented along the Y direction coincident with the b crystal axis.

The dipole moment distributions of uzonite-type and realgar-type molecules are shown in panels e and f of Figure 5, respectively. The two distributions arise from the variations of the molecular dipole moment as a consequence of thermal distortions of the cages during the CPMD simulation. The average values of the distributions along with the standard deviations are reported in Table 1 (column D).
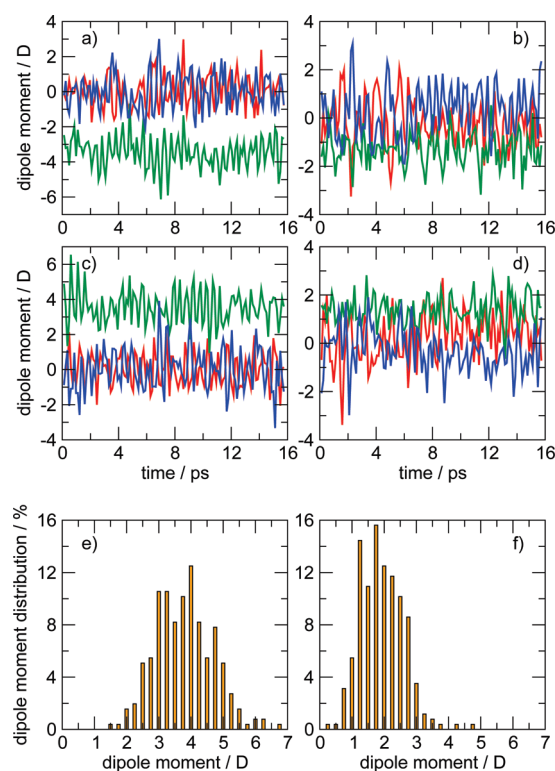

Figure 5. Dipole moment variations along the X (red), Y (green), and Z (blue) directions; panels a and c refer to the uzonite-type As_4S_5 molecules, while panels b and d refer to the realgar-type As_4S_4 molecules in the primitive cell of alacranite. The dipole moment distribution for uzonite-type As_4S_5 and realgar-type As_4S_4 molecules are reported in panels e and f, respectively.

Although the stability of the arsenic sulfide crystals is usually attributed to the van der Waals forces,[5,14] these results show that the presence in alacranite of As_4S_5 molecules, which are characterized by a permanent dipole moment, allows permanent dipole—dipole and permanent dipole—induced dipole interactions, which increase the stabilization due to the electrostatic terms.

Additional information on the interactions between realgar- and uzonite-like cages in the crystal can be recovered by the analysis of the Raman spectrum of the mineral. The frequency positions and the relative intensities of the Raman bands in the region between 215 and 500 cm^{-1} (Figure 6a) are correctly reproduced by the calculations (Figure 6b), with the exception of that observed at $\sim$220 cm^{-1}, whose intensity is slightly overestimated. The calculated Raman spectrum of the crystal has been obtained by computing the polarizability tensor on equispaced configurations of the CPMD simulation, adopting the generalized variational density functional perturbation theory,[24] recently extended to any simulation cell shape.[23]

Partitioning the polarizability tensor in the isotropic (α_{iso}) and anisotropic (α_{aniso}) parts,[45]

$$\alpha(t) = \alpha_{iso}(t) + \alpha_{aniso}(t) = \frac{1}{3}\mathrm{Tr}\alpha(t) + \alpha_{aniso}(t) \quad (1)$$

the Raman intensities, $I(\omega)$, can be obtained as

$$I(\omega) = \frac{\beta\hbar\omega}{1 - e^{-\beta\hbar\omega}}\big[\mathscr{F}(\alpha_{iso}(t))\mathscr{F}^*(\alpha_{iso}(t))$$
$$+ \frac{4}{30}\mathscr{F}(\mathrm{Tr}[\alpha_{aniso}](t))\mathscr{F}^*(Tr[\alpha_{aniso}](t))\big] \quad (2)$$
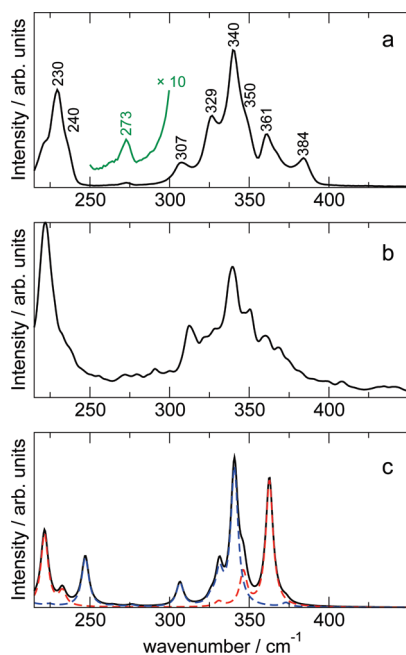
Figure 6. (a) Observed Raman spectrum of alacranite. The principal spectral features have been identified by the corresponding wavenumbers. The green trace enhances the band at 273 cm^{-1} attributable to pararealgar. (b) Calculated Raman spectrum of the alacranite crystal. The frequencies have been uniformly scaled by 1.105. (c) Calculated Raman spectrum (black line) as a sum of those corresponding As$_4$S$_4$ (red line) and As$_4$S$_5$ (blue line) isolated molecules. The calculated spectra (BLYP/6-311++G(d,p) using the Gaussian 03 suite of programs[46] in panel c were reported by assigning to each normal mode a Lorentzian shape with a 5 cm^{-1} full width at half-maximum. The frequencies have been uniformly scaled by 1.08.

where ω is the frequency of the scattered light, $\beta = 1/(k_{\mathrm{B}}T)$, and $\mathscr{F}$ is the Fourier transform.

With the comparison of panels b and c of Figure 6 with Figure 6a, it can be noted that the Raman spectrum obtained as a sum of the contributions of the As$_4$S$_4$ and As$_4$S$_5$ isolated molecules (Figure 6c) does not correctly reproduce the experiment. In particular, the band intensities of the realgar-type cage appear largely overestimated with respect to the observed values. This result confirms that the intermolecular interactions play an important role not only on the stability of the mineral but also on the spectroscopic properties. However, the calculated Raman bands of the isolated arsenic sulfide molecules (blue and red dashed traces of Figure 6c) represent a reliable help for the correct interpretation of the observed bands. The presence of a small amount of pararealgar[13] is revealed by the observation of a very weak band at 273 cm^{-1}.

Figure 7 shows the normal modes of As$_4$S$_4$ and As$_4$S$_5$ molecules, along with a tentative assignment of the prominent Raman bands reported in Figure 6a.

The Raman spectrum in Figure 6a can be divided into two regions related to the vibrational modes with most contributions from Cartesian displacements of arsenic and sulfur atoms, respectively, as reported in Figure 7. In this respect, the arsenic region is characterized by the breathing modes of As$_4$S$_4$ and As$_4$S$_5$ cages at 230 and 240 cm^{-1}. The corresponding breathing modes in the sulfur region have been instead observed at 340 cm^{-1} for the uzonite-like cage and at 361 cm^{-1} for the realgar-like cage. The
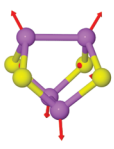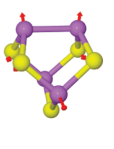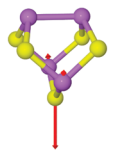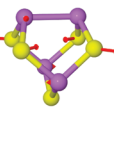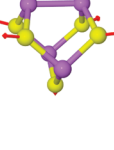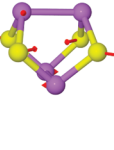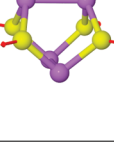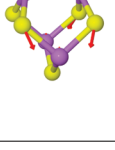

Figure 7. Graphical representation of the normal modes of As$_4$S$_4$ and As$_4$S$_5$ cages with their symmetries, corresponding to the observed Raman bands of alacranite. Yellow and violet spheres refer to sulfur and arsenic atoms, respectively; breath. = breathing mode; def. = deformation mode.

relative intensities of these modes computed in the crystal substantially differs from those obtained for the isolated molecules, showing a much better agreement with the experiments. This behavior can be attributed to the different interactions of the As$_4$S$_4$ cages in alacranite with respect to realgar crystal, where the breathing band occurs[12,13] at 355 cm^{-1} as the most intense. The normal mode at 307 cm^{-1} is characterized by the displacement of one sulfur atom (S(1) in Figure 1c) of the uzonite-like molecule, whereas the motion of the other four sulfur atoms (S(2) in Figure 1c) is involved in the deformation mode observed at 384 cm^{-1}. The bands at 329 and 350 cm^{-1} have been, instead, assigned to different deformation modes of the As$_4$S$_5$ and As$_4$S$_4$ cages, respectively.

■ CONCLUSIONS

CPMD simulations performed on the alacranite crystal have revealed it to be particularly suitable for reproducing the structural properties. This result is important to understand the

D

dx.doi.org/10.1021/jp201097k |J. Phys. Chem. A XXXX, XXX, 000–000

interactions that take place in crystals, characterized by the presence of molecules with different composition and electronic structure. The intermolecular electrostatic interactions in alacranite are more significant than in realgar owing to the presence of a permanent dipole moment in the As_4S_5 cage-like molecule, strongly affecting the spectroscopic properties. As a confirmation, the Raman spectrum of alacranite has been correctly reproduced only by the calculations on the crystal, where intermolecular interactions are directly computed from first principles.

■ AUTHOR INFORMATION

Corresponding Author

*E-mail: gianni.cardini@unifi.it.

■ ACKNOWLEDGMENT

■ REFERENCES

(1) McMillan, P. F. *Annu. Rev. Earth Planet. Sci.* **1989**, *17*, 255–283.

(2) Trentelman, K.; Stodulski, L.; Pavlosky, P. *Anal. Chem.* **1996**, *68*, 1755–1761.

(3) Bindi, L.; Popova, V.; Bonazzi, P. *Can. Mineral.* **2003**, *41*, 1463–1468.

(4) Bonazzi, P.; Bindi, L.; Pratesi, G.; Menchetti, S. *Am. Mineral.* **2006**, *91*, 1323–1330.

(5) Bonazzi, P.; Bindi, L. *Z. Kristallogr.* **2008**, *223*, 132–147.

(6) Naumov, P.; Makreski, P.; Jovanovski, G. *Inorg. Chem.* **2007**, *46*, 10624–10631.

(7) Naumov, P.; Makreski, P.; Petrusevski, G.; Runcevski, T.; Jovanovski, G. *J. Am. Chem. Soc.* **2010**, *132*, 11398–11401.

(8) Kyono, A.; Kimata, M.; Hatta, T. *Am. Mineral.* **2005**, *90*, 1563–1570.

(9) Kyono, A. *J. Photochem. Photobiol., A: Chem.* **2007**, *189*, 15–22.

(10) Ballirano, P.; Maras, A. *Eur. J. Mineral.* **2006**, *18*, 589–599.

(11) Douglass, D. L.; Shing, C.; Wang, G. *Am. Mineral.* **1992**, *77*, 1266–1274.

(12) Bonazzi, P.; Menchetti, S.; Pratesi, G.; Muniz-Miranda, M.; Sbrana, G. *Am. Mineral.* **1996**, *81*, 874–880.

(13) Muniz-Miranda, M.; Sbrana, G.; Bonazzi, P.; Menchetti, S.; Pratesi, G. *Spectrochim. Acta A* **1996**, *52*, 1391–1401.

(14) Gibbs, G. V.; Wallace, A. F.; Downs, R. T.; Ross, N. L.; Cox, D. F.; Rosso, K. M. *Phys. Chem. Minerals* **2011**, *38*, 267–291.

(15) Bonazzi, P.; Bindi, L.; Popova, V.; Pratesi, G.; Menchetti, S. *Am. Mineral.* **2003**, *88*, 1796–1800.

(16) Porter, E. J.; Sheldrick, G. M. *J. Chem. Soc., Dalton Trans.* **1972**, 1347–1349.

(17) Mullen, D. J. E.; Nowacki, W. *Z. Kristallogr.* **1972**, *136*, 48–65.

(18) Whitfield, H. J. *J. Chem. Soc., Dalton Trans.* **1973**, 1740–1742.

(19) Car, R.; Parrinello, M. *Phys. Rev. Lett.* **1985**, *55*, 2471–2474.

(20) Parrinello, M. *Solid State Commun.* **1997**, *102*, 107–120.

(21) Tse, J. S. *Annu. Rev. Phys. Chem.* **2002**, *53*, 249–290.

(22) Marx, D.; Hutter, J. *Ab Initio Molecular Dynamics: Basic Theory and Advanced Methods*; Cambridge University Press: Cambridge, U.K., 2009.

(23) Pagliai, M.; Cavazzoni, C.; Cardini, G.; Erbacci, G.; Parrinello, M.; Schettino, V. *J. Chem. Phys.* **2008**, *128*, 224514.

(24) Putrino, A.; Sebastiani, D.; Parrinello, M. *J. Chem. Phys.* **2000**, *113*, 7102–7109.

(25) CPMD. Copyright IBM Corp. 1990−2008, Copyright MPI für Festkörperforschung Stuttgart 1997−2001. http://www.cpmd.org.

(26) Becke, A. D. *Phys. Rev. A* **1988**, *38*, 3098–3100.

(27) Lee, C.; Yang, W.; Parr, R. G. *Phys. Rev. B* **1988**, *37*, 785–789.

(28) Goedecker, S.; Teter, M.; Hutter, J. *Phys. Rev. B* **1996**, *54*, 1703–1710.

(29) Hartwigsen, C.; Goedecker, S.; Hutter, J. *Phys. Rev. B* **1998**, *58*, 3641–3662.

(30) Krack, M. *Theor. Chem. Acc.* **2005**, *114*, 145–152.

(31) Monkhorst, H. J.; Pack, J. D. *Phys. Rev. B* **1976**, *13*, 5188–5192.

(32) Grimme, S. *J. Comput. Chem.* **2006**, *27*, 1787–1799.

(33) Margenau, H.; Kestner, N. R. *Theory of Intermolecular Forces*; Pergamon Press: Oxford, U.K., 1969.

(34) Marzari, N.; Vanderbilt, D. *Phys. Rev. B* **1997**, *56*, 12847–12865.

(35) Berghold, G.; Mundy, C. J.; Romero, A. H.; Hutter, J.; Parrinello, M. *Phys. Rev. B* **2000**, *61*, 10040–10048.

(36) Silvestrelli, P. L.; Parrinello, M. *Phys. Rev. Lett.* **1999**, *82*, 3308–3311.

(37) Silvestrelli, P. L.; Parrinello, M. *J. Chem. Phys.* **1999**, *111*, 3572–3580.

(38) Boero, M.; Terakura, K.; Ikeshoji, T.; Liew, C. C.; Parrinello, M. *Phys. Rev. Lett.* **2000**, *85*, 3245–3248.

(39) Boero, M.; Terakura, K.; Ikeshoji, T.; Liew, C. C.; Parrinello, M. *J. Chem. Phys.* **2001**, *115*, 2219–2227.

(40) Boero, M.; Parrinello, M.; Terakura, K.; Ikeshoji, T.; Liew, C. C. *Phys. Rev. Lett.* **2003**, *90*, 226403.

(41) Sharma, M.; Resta, R.; Car, R. *Phys. Rev. Lett.* **2005**, *95*, 187401.

(42) Scipioni, R.; Schmidt, D. A.; Boero, M. *J. Chem. Phys.* **2009**, *130*, 024502.

(43) Pagliai, M.; Cardini, G.; Righini, R.; Schettino, V. *J. Chem. Phys.* **2003**, *119*, 6655–6662.

(44) Handgraaf, J.-W.; van Erp, T. S.; Meijer, E. *J. Chem. Phys. Lett.* **2003**, *367*, 617–624.

(45) Berne, B. J.; Pecora, R. *Dynamic Light Scattering*; John Wiley & Sons, Inc.: New York, 1976.

(46) Frisch, M. J. et al.; *Gaussian 03*; Revision C.02; Gaussian, Inc.: Wallingford CT, 2004.

E

dx.doi.org/10.1021/jp201097k |*J. Phys. Chem. A* XXXX, XXX, 000–000